

Insertion of a Two-Dimensional Iron-Chloride Network between Perovskite Blocks. Synthesis and Characterization of the Layered Oxyhalide, (FeCl)LaNb₂O₇

Liliana Viciu, Julien Koenig, Leonard Spinu, Weillie L. Zhou, and John B. Wiley*

Department of Chemistry and the Advanced Materials Research Institute, University of New Orleans, New Orleans, Louisiana 70148-2820

Received August 9, 2002. Revised Manuscript Received January 8, 2003

A low-temperature (350 °C) ion-exchange reaction was used to insert Fe–Cl layers between the perovskite blocks of a double-layered Dion–Jacobson compound. The product, (FeCl)LaNb₂O₇, contains iron coordinated by two apical oxygens from the perovskite layer and four in-plane chlorines within the interlayer space. Rietveld structural analysis of X-ray powder diffraction data confirms the formation of the two-dimensional iron–chlorine networks with the iron cations moving slightly off the ideal octahedral coordination. Thermal analyses in oxygen, argon, and hydrogen showed this compound is metastable, decomposing exothermically between 600 and 750 °C. Magnetic measurements show Curie–Weiss behavior at higher temperatures consistent with Fe²⁺ in a high-spin *d*⁶ configuration. At lower temperatures two transitions are observed: below 80 K an antiferromagnetic transition occurs, and below 10 K spins realign in a ferromagnetic fashion.

Introduction

Dion–Jacobson¹ A[A′_{n-1}B_nO_{3n+1}] and Ruddlesden–Popper² A₂[A′_{n-1}B_nO_{3n+1}] (A = alkali metal; A′ = alkaline earth metal or rare earth metal; B = transition metal; *n* ≥ 2) layered perovskites have been extensively investigated due to their ability to undergo topotactic manipulation.³ The fact that these materials have alkali ions weakly bound between the perovskite layers has been demonstrated through their receptiveness to ion exchange. In RbLaNb₂O₇ for example, Rb⁺ ion is readily replaced with NH₄⁺, H⁺, Na⁺, Li⁺, and Ag⁺.⁴ Recently, we⁵ and others⁶ have shown that combinations of cations and anions can be co-inserted into layered perovskites. In the case of metal halides, we have found that it is possible to make a series of copper–chloride and copper–bromide arrays within a number of Dion–Jacobson layered perovskites.⁵ The copper ions, in octahedral coordination, bridge between the apical oxide ions of the perovskite slabs while surrounded by four

halide ions. Most recently, we reported on our initial efforts in the synthesis of metal–chloride arrays with iron as well as other first-row transition metals.^{7,8} Herein we present a detailed study on the synthesis and characterization of (FeCl)LaNb₂O₇.

Experimental Section

Synthesis. The Dion–Jacobson phase, RbLaNb₂O₇, was prepared by a method similar to that reported in the literature.⁴ Initially, La₂O₃ was heated at 1050 °C for 16 h in order to remove any impurities such as carbonates or water. Then stoichiometric quantities of La₂O₃ (Alfa, 99.99%) and Nb₂O₅ (Alfa, 99.9985%) with a 25% molar excess of Rb₂CO₃ (Alfa, 99%) were ground together, annealed in an alumina crucible for 12 h at 850 °C and 24 h at 1050 °C. The excess of Rb₂CO₃ was added to balance that lost due to volatilization. The product was washed with distilled water and dried at 150 °C overnight. The cesium analogue was prepared by the same procedure as rubidium, starting from Cs₂CO₃ (Alfa, 99.994%). The other members of the series were obtained by ion exchange from RbLaNb₂O₇ and the corresponding nitrates in a 10:1 molar ratio. Different temperatures were used for the exchange depending of the melting point of the salt; the reaction temperature was 300 °C for LiLaNb₂O₇, 400 °C for NaLaNb₂O₇, and 350 °C for KLaNb₂O₇. After 24 h the products were thoroughly washed with warm water and acetone, dried at 150 °C for 4 h, and then examined by X-ray powder diffraction. In the K and Na compounds, single-phase products were best obtained after three similar treatment cycles with molten salt; the lithium compound was obtained in a single cycle. Although single-phase host compounds were often readily prepared by ion exchange from RbLaNb₂O₇, occasionally problems occurred

* To whom correspondence should be addressed. Phone: 504-280-6849. Fax: 504-280-6860. E-mail: jwiley@uno.edu.

(1) Dion, M.; Ganne, M.; Tournoux, M. *Mater. Res. Bull.* **1981**, *16*, 1429. (b) Dion, M.; Ganne, M.; Tournoux, M.; Ravez, J. *Rev. Chim. Miner.* **1984**, *21*, 92. (c) Jacobson, A. J.; Johnson, J. W.; Lewandowski, J. T. *Inorg. Chem.* **1985**, *24*, 3729.

(2) Ruddlesden, S. N.; Popper, P. *Acta Crystallogr.* **1957**, *10*, 538. Ruddlesden, S. N.; Popper, P. *Acta Crystallogr.* **1958**, *11*, 54.

(3) Schaak, R. E.; Mallouk, T. E. *Chem. Mater.* **2002**, *14*, 1455, and references therein.

(4) Gopalakrishnan, J.; Bhat, V.; Raveau, B. *Mater. Res. Bull.* **1987**, *22*, 413.

(5) Kodenkandath, T. A.; Lalena, J. N.; Zhou, W. L.; Carpenter, E. E.; Sangregorio, C.; Falster, A. U.; Simmons, W. B.; O'Connor, C. J.; Wiley, J. B. *J. Am. Chem. Soc.* **1999**, *121*, 10743. (b) Kodenkandath, T. A.; Kumbhar, A. S.; Zhou, W. L.; Wiley, J. B. *Inorg. Chem.* **2001**, *40*, 710.

(6) Gopalakrishnan, J.; Sivakumar, T.; Ramesha, K.; Thangadurai V.; Subbanna G. N. *J. Am. Chem. Soc.* **2000**, *121*, 6237.

(7) Kodenkandath, T. A.; Viciu, M. L.; Zhang, X.; Sims, J. A.; Gilbert, E. W.; Augrain, F.-X.; Chotard, J.-N.; Caruntu, G. A.; Spinu, L.; Zhou, W. L.; Wiley, J. B. *Proc. Mater. Res. Soc. Symp.* **2001**, *658*, GG8.5.1.

(8) Viciu, L.; Caruntu, G.; Royant, N.; Koenig, J.; Zhou, W. L.; Kodenkandath, T. A.; Wiley, J. B. *Inorg. Chem.* **2002**, *41*, 3385.

Table 1. Reaction Times for the Preparation of (FeCl)LaNb₂O₇ from Various Hosts

host	LiLaNb ₂ O ₇	NaLaNb ₂ O ₇	KLaNb ₂ O ₇	RbLaNb ₂ O ₇	CsLaNb ₂ O ₇
reaction time	2 days	3–4 days	4 days	14 days	incomplete reaction after 18 days

– incomplete exchange, as indicated by residual rubidium in the elemental analysis, or the formation of a minor impurity, thought to be LaNbO₄.

(FeCl)LaNb₂O₇ was prepared by a single step ion-exchange reaction between anhydrous FeCl₂ (Alfa, 99.5%) and ALaNb₂O₇ (A = Li, Na, K, Rb, Cs). ALaNb₂O₇ was mixed with 2-fold molar excess of anhydrous iron chloride and then pressed into a pellet (~50 000 psi). To minimize air exposure during the pressing, the die was covered with Parafilm. The reaction was carried out in a sealed, evacuated (<10⁻³ Torr) Pyrex tube at 350 °C. After 14 days of annealing the sample was washed with water and acetone to eliminate the excess iron chloride and the rubidium chloride byproduct. The product was light brown. If the reactants are not anhydrous, black crystals of iron oxide form and ion exchange does not occur. Samples used in structural, thermal, and magnetic analysis were all made from RbLaNb₂O₇.

Ion exchange with FeBr₂ (Alfa, 98%) was also examined using the same processing regimen. When anhydrous FeBr₂ was combined with RbLaNb₂O₇, a dark green compound formed. Elemental analysis indicated the formation of Fe_{0.5}-LaNb₂O₇, showing that although ion exchange did occur, it involved only cation species.⁷

Characterization. The products were insoluble in a variety of acids even after exposure to acidic solutions for long periods of time. Elemental analysis was therefore carried out by energy dispersive spectroscopy (EDS) on a series of individual crystallites on a JEOL (model JSM-5410) scanning electron microscope (SEM) equipped with an EDAX (DX-PRIME) microanalytical system. The composition Fe/Cl/La/Nb of (FeCl)-LaNb₂O₇ prepared from RbLaNb₂O₇ was found to be 1.020(7):0.979(6):1.084(9):2; no residual rubidium was observed.

X-ray powder diffraction data were collected on a Philips X-Pert PW 3020 MPD X-ray diffractometer equipped with a graphite monochromator and Cu K α radiation ($\lambda = 1.5418 \text{ \AA}$). The patterns were recorded in step-scanning mode between 10 and 110° 2 θ with 0.02° step width and 10 s count time. Structure models were refined by the Rietveld method with the GSAS package.⁹ Forty-two parameters were varied including scale factor, zero-point shift, ten background parameters, fourteen peak shape parameters, cell parameters, atomic coordinates, site occupancies for iron and chlorine, and preferred orientation. The *R* factor (*R*_p), the weighted *R* factor (*R*_{wp}), and χ^2 are defined as the following: profile, $R_p = \sum |y_{io} - y_{ic}| / \sum y_{io}$; weighted profile, $R_{wp} = [\sum w_i (y_{io} - y_{ic})^2 / \sum w_i (y_{io})^2]^{1/2}$; and goodness of fit (GOF), $\chi^2 = [R_{wp} / R_{exp}]^2$. $R_{exp} = [(N - P) / \sum w_i y_{io}^2]^{1/2}$, y_{io} and y_{ic} are the observed and calculated intensities, w_i is the weighting factor, *N* is the total number of y_{io} data when the background is refined, and *P* is the number of adjusted parameters.

The stability of the product was investigated both by thermogravimetric analysis (TGA) on a TA Instruments Thermal Analyst-2000 system and by differential scanning calorimetry (DSC) with a Netzsch 404S instrument. Samples were heated to 1000 °C with a 10 °C/min ramp in reducing (8% hydrogen in argon), oxidizing (oxygen), and inert (argon) atmospheres. Additional information about thermal stability of the material was obtained by high-temperature X-ray powder diffraction (HTXRD) on an Anton Paar HTK16; samples were scanned from 10 to 60° 2 θ between 350 and 1000 °C in 50 °C increments.

Magnetic susceptibility measurements were carried out with a superconducting quantum interference device (SQUID) magnetometer (Quantum Design, MPMS-5S) over the temperature range 3–300 K in fields of 100 Oe and 10 000 Oe. Both field-cooled (FC) and zero-field-cooled (ZFC) data were

Table 2. Tetragonal Unit Cell Parameters for the Parent and the Exchange Product

compd	unit cell (Å)	cell vol (Å ³)
RbLaNb ₂ O ₇	<i>a</i> = 3.896(9) <i>c</i> = 11.027(2)	167.4
(FeCl)LaNb ₂ O ₇	<i>a</i> = 3.879(1) <i>c</i> = 11.861(5)	178.46

obtained. Measurements of ac susceptibility were performed on a physical properties measurement system (PPMS) ac/dc magnetometer option with an ac drive field of 10 Oe, oscillating at 0.1, 1.0, 5.0, and 10.0 kHz.

The heat capacity of the material was measured with a Quantum Design PPMS equipped with a heat capacity option in the 2–300 K temperature range both in the absence and presence of a magnetic field (1 T).

Results

Synthesis. The synthesis of (FeCl)LaNb₂O₇ was examined starting from each of the alkali metal Dion–Jacobson series, ALaNb₂O₇ (A = Li, Na, K, Rb, Cs). Single-phase materials were obtained at 350 °C, and it was observed that the reaction rate decreases going through the series from lithium to rubidium (Table 1). In the case of cesium, the reaction was incomplete even after 18 days. The chemical analysis of the carefully washed product showed no evidence of rubidium, and the Fe/Cl/La/Nb ratio was close to stoichiometric. An exception to this was sometimes seen in syntheses with A = Li, Na, or K precursors where trace amounts of residual rubidium were detected, due to incomplete exchange in the synthesis of the precursors from RbLaNb₂O₇. Compounds used in structural and properties measurements were all prepared from RbLaNb₂O₇.

Exchange reactions involving FeBr₂ did not show the same behavior as those with FeCl₂. Instead of the co-exchange of both metal and halide species, the two alkali metal cations were replaced with a single iron (II) cation. Elemental analysis established the composition of the product to be Fe_{0.5}LaNb₂O₇.

Structure. All the reflections in the (FeCl)LaNb₂O₇ powder pattern were indexed on a tetragonal cell (Table 2).¹⁰ An expansion in the *c* axis (ca. 0.84 Å) was observed relative to the RbLaNb₂O₇ precursor. The initial model used in Rietveld refinement was similar to that of (CuCl)LaNb₂O₇ where the transition metal sat in an octahedral site surrounded by two apical oxygens from the perovskite layer and four coplanar chlorines (space group *P4/mmm*).^{5,11} This model, however, resulted in large thermal parameters for both iron and chlorine ions. Several models that involved disorder were then investigated. The best appeared to be that in which the iron cation was moved off its ideal position (1/2, 1/2, 1/2) to the more general position (*x*, 1/2, 1/2) while the chlorine was left on the (0, 0, 1/2) site. The observed, calculated, and difference plots for the Rietveld refinement of

(10) When A is not rubidium in ALaNb₂O₇, an unindexed reflection was sometimes observed at approximately 29° 2 θ ; this reflection matches the strongest line for LaNbO₄. This phase forms as an impurity during the preparation of ALaNb₂O₇ from RbLaNb₂O₇.

(11) Caruntu, G.; Kodendath, T. A.; Wiley, J. B. *Mater. Res. Bull.* **2002**, *37*, 593.

(9) Larson, A.; Von Dreele, R. B. *GSAS: Generalized Structure Analysis System*; Los Alamos National Laboratory: Los Alamos, NM, 1994.

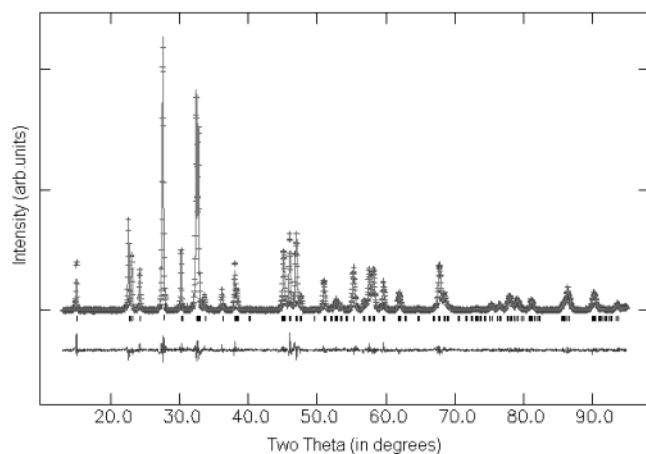


Figure 1. X-ray powder patterns for the Rietveld refinement of $(\text{FeCl})\text{LaNb}_2\text{O}_7$. Observed data are indicated by crosses and the calculated pattern is indicated by a solid line; the difference plot is shown at the bottom.

Table 3. Crystallographic Data for $(\text{FeCl})\text{LaNb}_2\text{O}_7^a$

atom	site	x	y	z	g	$U_{\text{iso}}(\text{\AA}^2)$
Fe	4o	0.421(2)	$1/2$	$1/2$	0.245(1)	0.007(2)
Cl	1b	0	0	$1/2$	0.969(8)	0.038(2)
La	1a	0	0	0	1	0.0137(4)
Nb	2h	$1/2$	$1/2$	0.19057(6)	1	0.0133(4)
O1	4i	0	$1/2$	0.1546(3)	1	0.018(1)
O2	2h	$1/2$	$1/2$	0.3358(5)	1	0.024(2)
O3	1c	$1/2$	$1/2$	0	1	0.016(3)

^a $P4/mmm$; $Z = 1$; $R_p = 10.28\%$; $R_{wp} = 15.44\%$; $\chi^2 = 1.612$; g = occupation factor.

Table 4. Selected Bond Distances for $(\text{FeCl})\text{LaNb}_2\text{O}_7$

bond	length (\AA)
Fe–O2 $\times 2$	1.972(6)
Fe–Cl $\times 2$	2.536(4)
$\times 2$	2.967(5)
Nb–O1 $\times 4$	1.986(1)
Nb–O2 $\times 1$	1.723(6)
Nb–O3 $\times 1$	2.260(1)
La–O1 $\times 8$	2.669(2)
La–O3 $\times 4$	2.742(1)

$(\text{FeCl})\text{LaNb}_2\text{O}_7$ based on this model are shown in Figure 1, and the corresponding structural parameters are presented in the Table 3. A slight deviation from stoichiometry for Fe and Cl in the structure was found. The structural model is shown in Figure 2. Selected bond distances are provided in Table 4 and these are consistent with literature values.¹²

Thermal Analysis. The stability of $(\text{FeCl})\text{LaNb}_2\text{O}_7$ was studied as a function of temperature in oxygen, argon, and hydrogen. TGA showed that $(\text{FeCl})\text{LaNb}_2\text{O}_7$ readily decomposes in all three atmospheres, and XRD analysis of the decomposition products found the formation of LaNbO_4 and either FeNb_2O_6 or FeNbO_4 depending on the atmosphere (Table 5). Interestingly, EDAX showed the complete absence of chlorine in all three samples and a significant loss of iron in the hydrogen treated sample. An exotherm in the DSC corresponds with the decomposition seen in TGA; the transition temperature of the exotherm is found to vary with atmosphere (Figure 3). Variable-temperature XRD in argon indicated that structural changes begin at ca. 500

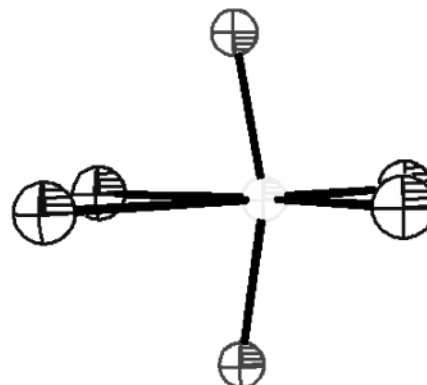
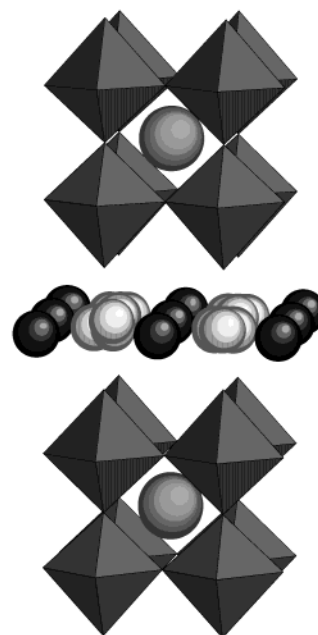


Figure 2. Top: structure of $(\text{FeCl})\text{LaNb}_2\text{O}_7$, the lightest spheres are the disordered iron cations, the darkest spheres are chlorines, and the medium gray spheres are lanthanums. The octahedra represent NbO_6 . Bottom: asymmetrical environment of the iron ion in the interlayer space of $(\text{FeCl})\text{LaNb}_2\text{O}_7$. The larger spheres represent chlorine.

Table 5. TGA Results for $(\text{FeCl})\text{LaNb}_2\text{O}_7$ in Different Atmospheres

atmosphere	weight loss (%)	final products
oxygen	4.218	LaNbO_4 , FeNbO_4
hydrogen	7.529	LaNbO_4 , FeNb_2O_6
argon	5.903	LaNbO_4 , FeNb_2O_6

$^\circ\text{C}$; the first decomposition product is $\text{Fe}_{0.5}\text{LaNb}_2\text{O}_7$, and above the exotherm transition temperature FeNbO_4 and FeNb_2O_6 were observed.

Magnetism. The variation in magnetic susceptibility as a function of temperature for $(\text{FeCl})\text{LaNb}_2\text{O}_7$ is shown in Figure 4. Measurements were performed at low (100 Oe) and high field (10 000 Oe). The compound is paramagnetic above 200 K and follows Curie–Weiss behavior (Figure 4a inset). The Curie–Weiss constant and the magnetic moment calculated from the fitted data are $\theta = -151.5$ K and $\mu_{\text{eff}} = 5.6 \mu_B$ per formula

(12) Wells, A. F. *Structural Inorganic Chemistry*, 5th ed.; Oxford University Press: New York, 1984.

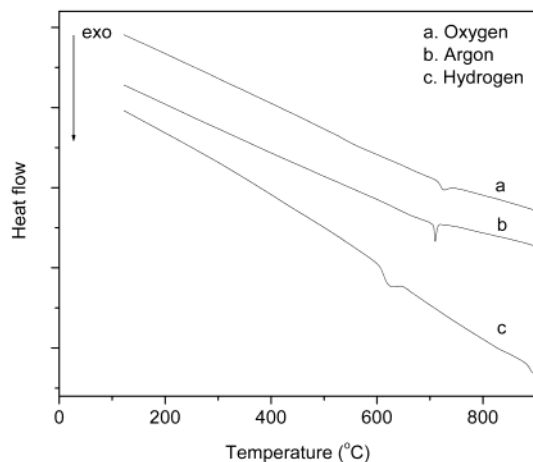
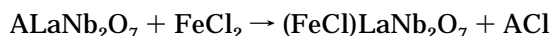


Figure 3. DSC curves for (FeCl)LaNb₂O₇ in oxygen, argon, and hydrogen.

unit of (FeCl)LaNb₂O₇, respectively. The moment is in agreement with those reported in the literature for ions in a high spin d^6 configuration.¹³ In an applied field of 100 Oe, the compound exhibits two maxima below 100 K: one at 87 K and another one at 8 K. Although both were observed in all samples measured at low fields, a slight variation in the relative magnitude of the two events was sometimes apparent. At higher fields (1 T), the lower temperature transition was suppressed (Figure 4b) and the ZFC and FC curves were equivalent. The magnetization versus magnetic field data measured at 70 and 300 K showed no hysteresis, whereas data taken at 5 and 15 K indicated a small coercive field, 120 and 60 Oe, respectively. The compound was also examined by ac susceptibility at several frequencies (Figure 5). The real part (χ') of the ac susceptibility was identical to the dc susceptibility data and showed no frequency dependence. In the imaginary part (χ''), however, only the low-temperature transition was observed; no frequency dependence was observed here as well. Heat capacity measurements were carried out in the presence and absence of a magnetic field (1 T); in both cases a transition was observed at 78 K (Figure 6). A plot of $\delta(\chi T)/\delta T$ versus T for the susceptibility data was made for the data to account for the offset between magnetic and heat capacity data;¹⁴ this also indicated a transition of 78 K.

Discussion

The synthesis of (FeCl)LaNb₂O₇ appears to go by a simple ion exchange reaction involving the replacement of the alkali metal cation (A) of the host, ALaNb₂O₇, by Fe²⁺ and Cl⁻.



Both diffusion relative to the reaction interface and cation mobilities within the host itself are expected to be important. In the case of the ACl-FeCl₂, much is known about their phase diagrams. As would be expected, eutectics readily form for each of the series with the lowest eutectic point occurring at 520, 370, 355, 458, and 499 °C for A = Li, Na, K, Rb, and Cs, respectively;¹⁵

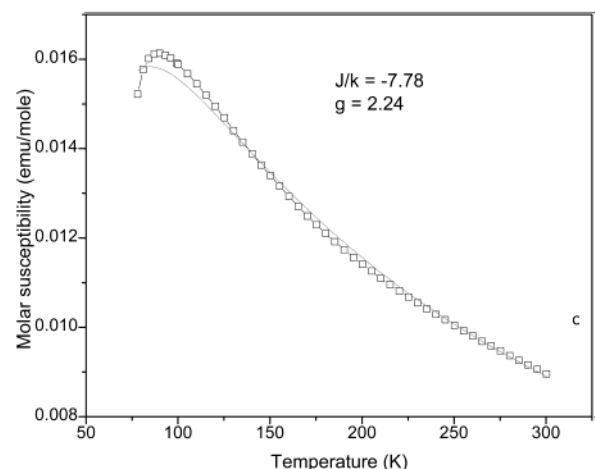
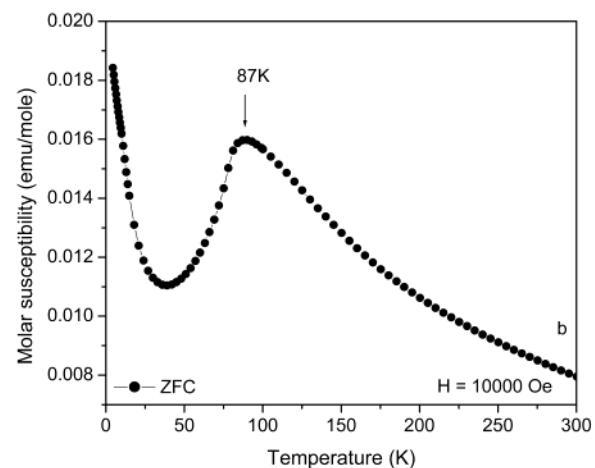
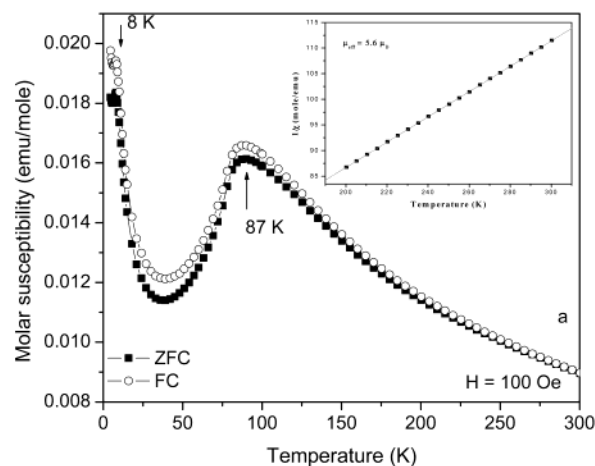


Figure 4. Temperature dependence of the magnetic susceptibility at (a) 100 Oe and (b) 10 000 Oe for (FeCl)LaNb₂O₇. (For 10 000 Oe only ZFC is shown – here ZFC and FC curves were equivalent.) The inset is the reciprocal molar susceptibility between 200 and 300 K. (c) Results of fitting (the solid line) a high-temperature series expansion of the quadratic layer Heisenberg model to the ZFC data at 100 Oe in 78–300 K range.

the ion exchange reactions were carried out at 350 °C, so that the movement of the reactants to, and the

(13) O'Connor, C. J. *Prog. Inorg. Chem.* **1982**, 29, 203.

(14) Fisher, M. *Philos. Mag.* **1962**, 7, 1731.

(15) Levin, E. M.; Robbins, C. R.; McMurdie, H. F. *Phase Diagrams for Ceramists, Volume I*; The American Ceramic Society: Columbus, OH, 1964, and Levin, E. M.; Robbins, C. R.; McMurdie, H. F. *Phase Diagrams for Ceramists, Volume II*; The American Ceramic Society: Columbus, OH, 1969.

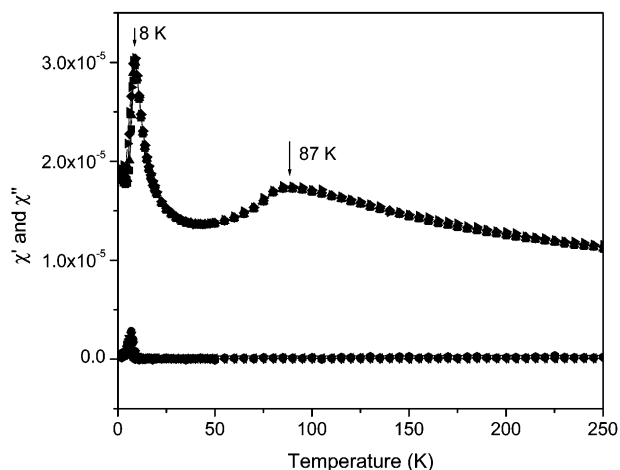


Figure 5. Alternating current (ac) susceptibility at 10 Oe with frequencies of 0.1, 1.0, 5.0, and 10.0 kHz. The top curve is the real component (χ') and the bottom curve is the imaginary component (χ'').

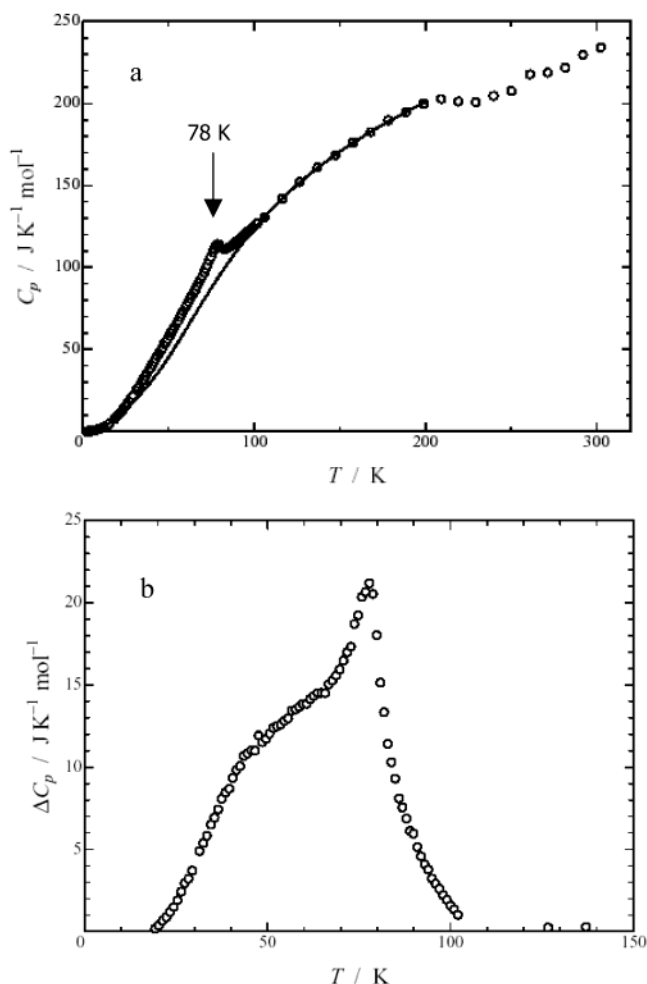


Figure 6. (a) Heat capacity as a function of temperature, $C_p(T)$, for $(\text{FeCl})\text{LaNb}_2\text{O}_7$. (b) Magnetic heat capacity as a function of temperature, $\Delta C_p(T)$, for $(\text{FeCl})\text{LaNb}_2\text{O}_7$.

byproducts away from, the surface of the host crystallites should be favorable in all these systems. Further, iron chloride itself is expected to have some vapor pressure under these reaction conditions, so that direct transport of gas species to the reaction interface is also possible.¹⁶ With respect to cation mobilities within the hosts, the alkali metal cation mobilities have been

investigated in some of the ALaNb_2O_7 as well as in other Dion–Jacobson type layered perovskites.¹⁷ Their mobilities are greater for the smaller alkali metals. With this in mind, the difference in reaction times seen for the series Li – Cs, appears to correlate well with the cation mobilities, indicating that the exchange step, not the diffusion of reactants to and products away from the reaction interface, is the limiting factor in these reactions.

The structure of the $(\text{FeCl})\text{LaNb}_2\text{O}_7$ is very similar to that of $(\text{CuCl})\text{LaNb}_2\text{O}_7$.^{5,11} The perovskite layers are maintained on ion exchange and the transition metal cations bridge between apical oxygens from the perovskite layers while surrounded by four coplanar chlorines. There are, however, some differences between the two structures, specifically with respect to the coordination of the metal cation. In the case of copper the chlorides appear to disorder to produce 4 short (2 oxygen and 2 chlorines) and two long bonds, consistent with a Jahn–Teller distortion.¹¹ Whereas for iron, the metal itself appears to move off an ideal octahedral position, favoring a tetrahedral-like distortion. This effect could be akin to a lattice mismatch between the perovskite layers and the intermediate iron-chloride layers. Considering the crystallographic radii¹⁸ of six coordinate Fe^{2+} (0.92 Å) and Cl^- (1.67 Å) the ideal match for this bond would be about 2.59 Å. Because the unit cell values along the face diagonal ($\sqrt{2} \times a/2 = 2.75$ Å) are slightly larger than this, the iron cation may move to compensate for this difference.

Thermal analysis shows that $(\text{FeCl})\text{LaNb}_2\text{O}_7$ is a low-temperature phase where decomposition is found to start around 500 °C. Also, the exothermic signature observed in DSC indicates that the compound is metastable. The heat released in this reaction may come from the formation of LaNbO_4 on decomposition of the perovskite layer; the coordination for lanthanum and niobium change from 12 and 6 to 8 and 4, respectively. In any case, these results indicate that $(\text{FeCl})\text{LaNb}_2\text{O}_7$ is not accessible by standard ceramic techniques.

The susceptibility and hysteresis data serve to illuminate the nature of the two magnetic transitions. The higher temperature transition with the drop in susceptibility at lower temperatures, the lack of hysteresis above and below the transition, and its absence in the χ'' data, all indicate that this transition corresponds to an antiferromagnetic (AFM) ordering of spins. Considering the two-dimensional structural features of this compound, efforts were made to model the dc susceptibility data between 78 and 300 K (Figure 4c) with the high-temperature series expansion reported by Rushbrooke and Wood¹⁹ for a 2D Heisenberg square planner system:

$$\chi = \frac{S(S+1)Ng^2\mu_B}{3kT} \sum_{n=0}^6 (-1)^n \left(\frac{b_n}{\theta^n} \right)$$

(16) Colton, R.; Canterford, J. H. *Halides of the First Row Transition Metals*; Wiley-Interscience: New York, 1969, and references therein.

(17) Sato, M.; Abo, J.; Jin, T.; Ohta, M. *J. Alloys Compd.* **1993**, *192*, 81.

(18) Shannon, R. D. *Acta Crystallogr.* **1976**, *A32*, 751.

(19) Rushbrooke, G. S.; Wood, P. *Mol. Phys.* **1963**, *6*, 409.

Table 6. Heat Capacity Parameters

	parameter (K)	degeneracy ^a
lattice vibrations	$\Theta_D = 107.6 \pm 1.3$	$3N_A$
molecular librations	$\Theta_E = 151 \pm 11$	$3N_A$
intramolecular vibrations	$\Theta_E = 310.5 \pm 1.3$	$20N_A$
	$\Theta_E = 965.7 \pm 3.8$	$10N_A$

^a N_A = degrees of freedom.

where N = Avogadro's number, k = Boltzmann constant, μ_B = Bohr magneton, $\theta = kT/J$, J = exchange constant, and the b coefficients were calculated to be $b_0 = 1$, $b_1 = -16$, $b_2 = 72$, $b_3 = -145.066$, $b_4 = 1781.866$, $b_5 = -10301.44$, and $b_6 = 14736.4266$. The value obtained for the exchange parameter is $J/k = -7.78$ K with $g = 2.24$. This result was further investigated by taking into account the maximum (χ_{\max}) of antiferromagnetic susceptibility using $kT(\chi_{\max})/|J|S(S+1)$ and $\chi_{\max}|J|Ng^2\mu_B^2$, where the theoretical values of these two terms for a square planar Heisenberg model with $S = 2$ are 2.07(1) and 0.0547(1), respectively.²⁰ Values calculated from these expressions for the intraplanar exchange constant (J/k) are 1.93 and 0.047, respectively. The difference attained between theoretical and calculated values together with the dissimilarity observed between the experimental curve and the calculated one in the vicinity of maximum susceptibility (Figure 4c) suggests that the chosen model is not the best one. Efforts to fit these data to an Ising model were also less than desirable. It is well-known that for high spin Fe²⁺ compounds, spin-orbit coupling and crystal distortions give rise to substantial anisotropy, where it is very difficult to represent the magnetic properties accurately by using pure isotropic (Heisenberg) or anisotropic (Ising) models.²¹ Similar behavior has been reported for other compounds containing Fe²⁺ layers.²²

The magnetic entropy was extracted from the heat capacity data by fitting two temperature ranges, 5–19 K and 106–199 K, by a nonlinear least-squares method taking into account both Debye and Einstein functions.²³ The best fit was obtained with a Debye function describing the lattice vibrations, an Einstein function describing the molecular librations, and two Einstein functions for the intramolecular vibrations. The normal heat capacity curve is represented with a solid line in Figure 6a, and the derived parameters are listed in Table 6. The magnetic contribution to the heat capacity (Figure 6b) is then obtained by subtracting the calculated normal heat capacity curve from the observed data. A magnetic entropy of 13.74 J/K·mol is extracted from these data using the relation $S_M = \int_0^T \Delta C_p d(\ln T)$.²⁴ This value is in reasonable agreement with the theoretical total magnetic entropy of 13.38 J/K·

mole calculated from $R \ln(2S + 1)$ for a system with $S = 2$.

The transition observed in the heat capacity data is consistent with magnetic ordering. The difference in the maximum temperature of the susceptibility data vs heat capacity data results from short range order magnetic interactions. In contrast, the lower temperature transition appears to correspond to ordered spins with a net magnetic moment; the difference between FC and ZFC data, the observed hysteresis above and below the transition, and the χ'' data all suggest a ferromagnetic transition. Heat capacity data in this case do not show a corresponding transition for the low-temperature event.

The relationship between the high- and low-temperature magnetic transitions is not clear at this point. On the basis of our analyses, all data indicate that the samples are single phase, so we do not believe that either of these transitions is associated with an impurity. It is likely that the AFM ordering arises from a superexchange mechanism between adjacent Fe²⁺ cations via bridging chloride ions. Similar broad AFM transitions have been observed previously in layered compounds and have been associated with short-range order within a plane.²¹ What comes into question is the origin of the low-temperature transition and its relationship to the AFM one. The lack of a second endotherm in the heat capacity data would be consistent with a reorientation of coupled spins. One possibility could be that the transition corresponds to the formation of a canted ferromagnet.²⁴ A detailed study of the magnetic structure of this system above and below both transitions would help to clarify these features. Efforts to perform a variable temperature neutron study are underway.

Conclusions

(FeCl)LaNb₂O₇ is a low-temperature, metastable phase that exhibits interesting structural and magnetic behavior. The unique properties offered by such systems emphasize the utility of low-temperature topotactic reactions for producing unusual new compounds. Especially exciting is the general prospect of topotactic strategies, where so-called "rational" syntheses could be used to access fundamentally and technologically important materials.

Acknowledgment. We gratefully acknowledge financial support from the National Science Foundation (DMR-9983591) and the Department of Defense (DAR-PA MDA972-97-1-0003). Further, we thank Quantum Design for carrying out the heat capacity measurements and M. Sorai and Y. Miyazaki for their extensive assistance in fitting the heat capacity data.

CM0208253

(20) de Jongh, L. J.; Miedena, A. R. *Adv. Phys.* **1974**, *23*, 1.

(21) Navarro, R. In *Magnetic Properties of Layered Transition Metal Compounds*; de Jongh, L. J., Ed.; Kluwer Academic Publishers: Dordrecht, The Netherlands, 1990; p 105, and references therein.

(22) Bellitto, C.; Federici, F.; Colapietro, M.; Portalone, G.; Caschera, D. *Inorg. Chem.* **2002**, *41*, 709. (b) Haynes, J. S.; Kosticas, A.; Sams J. R.; Simopoulos, A.; Thompson R. C. *Inorg. Chem.* **1987**, *26*, 2630.

(23) Kittel, C. *Introduction to Solid State Physics*, 7th ed; John Wiley & Sons: New York, 1996.

(24) Carlin, R. L. *Magnetochemistry*; Springer-Verlag: Berlin, 1986, and references therein.